# Valley Filtering and Electronic Optics Using Polycrystalline Graphene

V. Hung Nguyen,[1,*] S. Dechamps,[1] P. Dollfus,[2] and J.-C. Charlier[1]

[1]*Institute of Condensed Matter and Nanosciences, Université catholique de Louvain,*
*Chemin des étoiles 8, B-1348 Louvain-la-Neuve, Belgium*
[2]*Centre for Nanoscience and Nanotechnology, CNRS, Université Paris Sud, Université Paris-Saclay, 91405 Orsay, France*

In this Letter, both the manipulation of valley-polarized currents and the optical-like behaviors of Dirac fermions are theoretically explored in polycrystalline graphene. When strain is applied, the misorientation between two graphene domains separated by a grain boundary can result in a mismatch of their electronic structures. Such a discrepancy manifests itself in a strong breaking of the inversion symmetry, leading to perfect valley polarization in a wide range of transmission directions. In addition, these graphene domains act as different media for electron waves, offering the possibility to modulate and obtain negative refraction indexes.

Because of its peculiar electronic structure and outstanding properties, graphene has become a material of choice for many fundamental research projects and promising applications [1,2]. The attractiveness of graphene lies basically in its massless Dirac fermions, high carrier mobility, small spin-orbit coupling, optical transparency, superior mechanical properties, and so on. Several fascinating phenomena (e.g., Klein tunneling, anomalous quantum Hall effect, Berry's phase manifestation, etc.) have been explored [1]. Graphene also turns out to be very promising for integration into a variety of electrical, spintronic, optical applications, flexible electronics, and so on [2]. Especially, two unconventional concepts, valleytronics and electronic optics, have been explored and rapidly attracted a great amount of attention from various scientific communities; see, e.g., Ref. [3] and references therein.

Valleytronics [4] lies in exploiting the feature that charge carriers flow through graphene as a wave populating the $K$ and $K'$ valleys [1] in its Brillouin zone, with each valley being characterized by a distinct momentum and a valley index [5,6]. In analogy with spintronics, manipulating carriers in these two valleys can be used to encode data, i.e., to represent the zeroes and ones in digital computing. To date, many strategies [5–9] have been proposed to break the valley degeneracy for creating and detecting the valley polarization in graphene. They mainly rely on the valley filtering effects and/or the generation of spatially separated valley-resolved currents in graphene nanostructures. Most remarkably, recent experimental advances have successfully demonstrated the electrical generation and control of pure valley current in graphene systems where the inversion symmetry is broken by a gap-opening perturbation [10,11].

The high mobility of carriers in graphene allows for ballistic transport over micrometer length scales even at room temperature [12]. Hence, electrons can flow in straight-line trajectories and their wave nature can manifest in a variety of interference and diffraction effects [13], in analogy with light rays in optical media. This makes graphene an ideal platform for demonstrating electronic optics and hence for developing novel quantum devices [14–19]. In this respect, the advantages of graphene also come from peculiar properties as low-energy linear dispersion with electron-hole symmetry, gapless character, and excellent gate controllability [17–19]. Because of the specific electronic dispersion, the group velocity of electrons (holes) in graphene is parallel (antiparallel) to their momentum. This results in negative refraction, a striking feature of electronic optics, when carriers transmit across graphene *p-n* junctions [14,19]. The gapless character makes graphene nanostructures highly transparent [15] while the gate controllability offers possibilities of electrically modulating the refraction index in electronic-optics components [16–19].

However, for practical applications, graphene samples synthesized at large scale (e.g., by CVD) are always found to be polycrystalline in nature [20–22], i.e., composed of different single-crystal grains separated by grain boundaries (GBs). This defective nature strongly affects the intrinsic properties of graphene [21,22]. Nevertheless, polycrystalline graphene can also offer opportunities of tailoring the electronic properties of domains so as to achieve desirable properties of the global system [21–30]. In this respect, several experiments have been conducted to characterize and control individual grains and grain boundaries, allowing for both intra- and intergrain transport measurements [23–26]. In the same direction, it has been predicted that besides being affected by the defect scattering [23], the transport through polycrystalline graphene strongly depends on the symmetry properties of its domains, which could be exploited to tune and achieve a metal-semiconductor transition [29,30]. In particular, if single-crystal domains are arranged in different

orientations, a mismatch of their electronic structures can occur, and hence a finite energy gap of conductance (transport gap) opens [29]. Actually, this gap is not an electronic band gap of graphene; i.e., it is achieved though the single-crystal domains remain semimetallic. The misorientation between these domains also offers the opportunity to modulate the transport gap by strain engineering [30].

In this Letter, a new and practical scheme is proposed to manipulate highly valley-polarized currents and optical-like behaviors of charge carriers in graphene, which are essential ingredients for valleytronics and electronic-optics applications. The approach lies in the use of polycrystalline graphene systems containing two misoriented domains separated by a GB that is composed of a periodic array of dislocations [see the examples in Figs. 1(a) and 1(b)]. In principle, these two domains exhibit different electronic structures, especially when the system is strained. Such a discrepancy is expected to manifest itself in a strong breaking of the inversion symmetry of the system, and hence a high valley polarization can be achieved. Additionally, in analogy to optical systems, these domains act as different media for electron waves, leading to optical-like behaviors of charge transport through the system. It is worth noting that this general approach can be extended to several polycrystalline systems of other materials that, similarly, contain different crystalline domains; see, e.g., Refs. [31,32].

Our investigation was conducted using atomistic simulations described in Ref. [30]. Considered graphene systems contain two commensurable domains separated by a periodic GB along the $y$ axis [see two examples in Figs. 1(a) and 1(b)]. The atomistic geometry of the system was relaxed using molecular dynamics to minimize its



FIG. 1.    Atomistic structure of graphene grain boundary systems (a) $(2,1)|(1,2)$ and (b) $(0,7)|(3,5)$. Charge carriers transmitted across the boundary under a uniaxial strain of magnitude $\sigma$ and direction $\theta$ are considered. (c) Diagrams illustrating the strain effects on the band structure of graphene domains (left) and the momentum conservation rule (right).

energy determined from optimized Tersoff potentials [33]. A uniaxial strain is applied with magnitude $\sigma$ and direction $\theta$ [see the inset of Figs. 1(a) and 1(b)]. The transport across the GB was computed using the Green's function method to solve the tight-binding model that has been empirically constructed to include the effects of strain [34,35].

Generally, charge transport through graphene-GB systems can be easily modulated by strain. Indeed, when strain is applied, Dirac cones (or valleys) $D$ and $D'$ of graphene are displaced and no longer located at the $K$ and $K'$ points [34]. Most importantly, misoriented domains show different responses to strain, leading to a separation of their Dirac cones in the $k$ space. Without any additional scattering, the charge transport satisfies the conservation of momentum $k_y$. The misalignment of Dirac cones hence results in a finite transport gap, which has been shown to be a function of strain ($\sigma$ and $\theta$) and lattice symmetry [30]. Let us now consider a de Broglie wave of electron approaching the GB from the left domain, which is characterized by velocity $\mathbf{v}_1 = v_1(\cos\phi_1, \sin\phi_1)$ and momentum $\mathbf{k}_1 = \mathbf{D}_1 + \mathbf{q}_1$, where $\mathbf{q}_1 = q_1(\cos\phi_1, \sin\phi_1)$ and $\phi_1$ is the incident angle. At the GB, this wave is partly reflected to the state with $\mathbf{v}_1^r = v_1(-\cos\phi_1, \sin\phi_1)$ and partly transmitted to the state with $\mathbf{v}_2 = v_2(\cos\phi_2, \sin\phi_2)$ and $\mathbf{k}_2 = \mathbf{D}_2 + \mathbf{q}_2$ [$\mathbf{q}_2 = q_2(\cos\phi_2, \sin\phi_2)$] in the right domain [see Fig. 1(c)]. Because of the $k_y$ conservation, the equation $q_1\sin\phi_1 - q_2\sin\phi_2 = D_{2y} - D_{1y}$ is satisfied. A similar relationship is obtained for valley $D'$ with $D'_{2y} - D'_{1y} = -(D_{2y} - D_{1y})$. Under small strain, the difference of energy dispersion around the Dirac cones between the two graphene domains is negligible, leading to $q_1 \cong q_2 = q$. This work focuses on only small strains that are much lower than the band gap threshold $\sigma_{gt} \simeq 23\%$ [34]. The above equation for $\phi_{1,2}$ can be hence rewritten as

$$\sin\phi_1 - \sin\phi_2 = \eta_v\alpha(q), \qquad (1)$$

where $\alpha(q) = (D_{2y} - D_{1y})/q$ and $\eta_v = \pm 1$ for valleys $D$ and $D'$, respectively. Furthermore, the group velocity and momentum are parallel (antiparallel) for electrons (holes). Equation (1) has to be modified, i.e., changing the sign of the right-hand term, for holes. In addition, in graphene under small strain, the energy dispersion around Dirac points is still linear and can be described by $\varepsilon = \pm\hbar v_F q$ with $v_F \simeq 1 \times 10^6$ m/s [1]. Hence, Eq. (1) can apply to both electrons and holes by using $\alpha(q) = \hbar v_F(D_{2y} - D_{1y})/\varepsilon$. Note additionally that the similar separation of Dirac cones and hence the same refraction rule can be achieved in incommensurable systems without strain [29]. In such a case, the strain can also be used to modulate these transport properties of the system [30,35].

Clearly, Eq. (1) implies that transmission in the two valleys is modulated differently by strain. Simultaneously, it manifests itself in a new refraction rule, compared to the ordinary ones, i.e., $\sin\phi_2 = \pm(q_1/q_2)\sin\phi_1$, in graphene

doped structures [14,15]. Equation (1) is thus the key element of the current work, which can explain high valley polarization and optical-like behaviors of charge carriers presented below.

*Valley filtering effects.*—In Fig. 2, transmission functions $\mathcal{T}_{D,D'}$ in the two valleys and valley polarization $P_{\mathrm{val}} = (\mathcal{T}_D - \mathcal{T}_{D'})/(\mathcal{T}_D + \mathcal{T}_{D'})$ in the two graphene systems GB1 and GB2 [see Figs. 1(a) and 1(b)] are displayed as a function of incident angle $\phi_1$ for different applied strains. Without strain, similarly to the case of graphene systems containing a line defect [7], scattering at GBs is shown to modify differently the functions $\mathcal{T}_{D,D'}$, leading to a finite $P_{\mathrm{val}}$. However, a high $P_{\mathrm{val}}$ is obtained only for large incident angles. When strain is applied, gaps of $\mathcal{T}_{D,D'}$ open in different ranges of $\phi_1$ and hence $P_{\mathrm{val}}$ can be strongly enhanced. Indeed, in both systems GB1 and GB2, a perfect $P_{\mathrm{val}}$ can be achieved in wide ranges of $\phi_1$ when applying a reasonably large strain, i.e., as shown for $\sigma = 2\%$–$3\%$ in Fig. 2. Additionally, $P_{\mathrm{val}}$ can be also modulated by tuning carrier energy, as discussed below.

To clarify these properties, Eq. (1) is used to distinguish different transport regimes as illustrated in Fig. 1(c). The $k_y$ conservation implies that the transmission is nonzero only if the solution of Eq. (1) exists. The angle $\phi_1$ has thus to satisfy $\max[\eta_v\alpha(q)-1,-1]\leq\sin\phi_1\leq\min[\eta_v\alpha(q)+1,1]$. In the low-energy regime $|\varepsilon| < \varepsilon_1$ [i.e., $|\alpha(q)| > 2$] with $\varepsilon_1 = \hbar v_F|D_{2y} - D_{1y}|/2$, no angle $\phi_1$ satisfies the above condition and thus the system is totally reflective, corresponding to a transport gap. In the second regime $\varepsilon_1 \leq |\varepsilon| < \varepsilon_2$ [i.e., $1 < |\alpha(q)|\leq 2$] with $\varepsilon_2 = \hbar v_F|D_{2y} - D_{1y}|$, the transmission is found to be nonzero in finite ranges of $\phi_1$. In particular, to obtain nonzero transmission of electrons, $\phi_1$ has to satisfy $\alpha(q) - 1 \leq \sin\phi_1 \leq 1$ and

$-1 \leq \sin\phi_1 \leq 1 - \alpha(q)$ for valleys $D$ and $D'$, respectively. These two ranges are fully separated, i.e., $\phi_1 > 0$ and $\phi_1 < 0$, respectively. In such ranges, the transmission is allowed for only one valley, leading to perfect $P_{\mathrm{val}}$ as observed for $\sigma = 3\%$ in Fig. 2. The third regime is $|\varepsilon| \geq \varepsilon_2$, i.e., $|\alpha(q)| \leq 1$. In this regime, the ranges of $\phi_1$ allowing for finite $\mathcal{T}_{D,D'}$ are larger than those observed in the second one and can overlap. Similarly as above, outside the overlapped range of $\phi_1$, a perfect $P_{\mathrm{val}}$ is obtained. Otherwise, $P_{\mathrm{val}}$ has smaller values inside the overlapped range, as shown for $\sigma = 1\%$ and $2\%$ in Fig. 2.

*Optical-like behaviors of charge carriers.*—As mentioned earlier, Eq. (1) also implies that electrons transmitted across the system have optical-like behaviors with new refraction rules. The relationship between $\phi_{1,2}$ extracted from the data in Fig. 2 is displayed in Figs. 3(a) and 3(b). Note that without strain and/or in systems containing domains of the same orientation [7], $\alpha(q) = 0$ and hence $\phi_2 = \phi_1$. Otherwise, the refraction index can be easily modulated by strain and/or by varying carrier energy, i.e., $\sin\phi_2 = \sin\phi_1 - \eta_v\alpha(q)$. Indeed, for small strains (e.g., $\sigma = 1\%$ and $2\%$ here), both positive and negative refraction indexes are observed. Interestingly, when strain is large enough (i.e., $\sigma = 3\%$), the refraction index is negative in the full $\phi_{1,2}$ ranges of finite transmission. Actually, the former case (small strains) corresponds to the energy regime $|\varepsilon| \geq \varepsilon_2$ while the latter corresponds to $\varepsilon_1 \leq |\varepsilon| < \varepsilon_2$ discussed above. Moreover, due to the
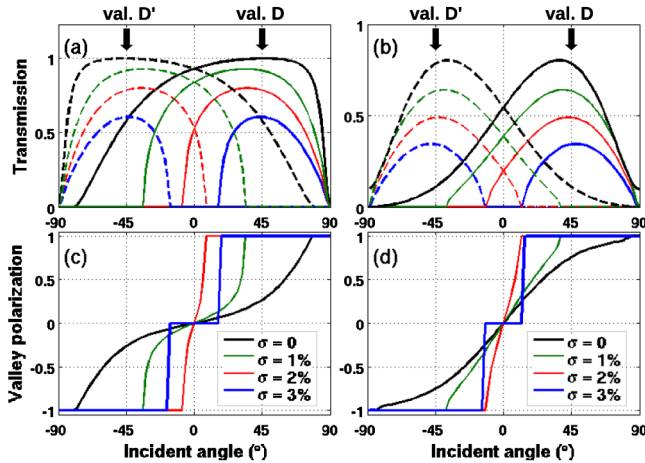


FIG. 2. (a),(b) Transmission probability in the two valleys and (c),(d) valley polarization as a function of incident angle for energy $\varepsilon = 0.3$ eV and different strains. (a),(c) and (b),(d) present the data obtained in the systems GB1 (for strain direction $\theta = 45°$) and GB2 (for $\theta = 22°$) in Figs. 1(a) and 1(b), respectively.
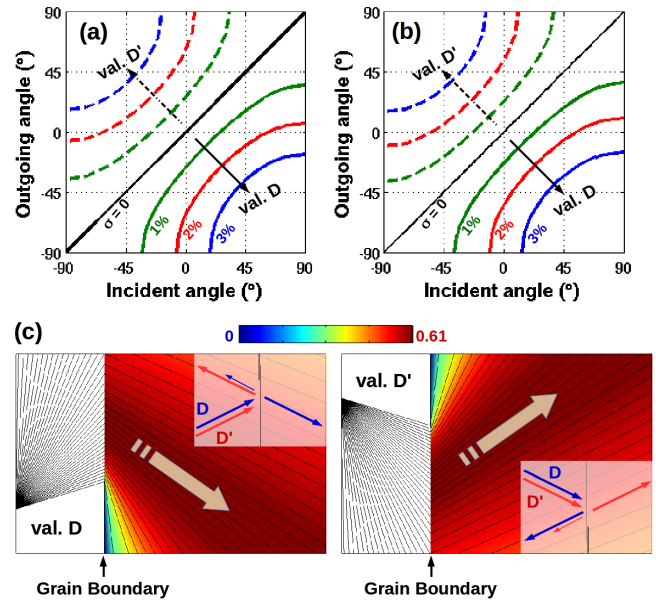


FIG. 3. Strain-induced modulation of refraction index in the (a) GB1 and (b) GB2 systems extracted from the data in Fig. 2. (c) Diagrams illustrating the properties of electron beams with negative refraction [particularly, for $\sigma = 3\%$ in (a)] and color maps showing the transmission function for different outgoing angles.

equivalence between $\phi_1$ and $-\phi_2$ in Eq. (1), the solutions of $\phi_{1,2}$ are symmetric with respect to $\phi = 0$.

Other novel properties are predicted as presented in Fig. 3(c). First, even being nonzero in a finite range of $\phi_{1,2}$, $\mathcal{T}_{D,D'}$ are numerically shown to be high only for directions around a specific angle satisfying $\phi_2 \cong -\phi_1 = -\phi_h$ where $\phi_h = \eta_v \arcsin[\alpha(q)/2]$. This angle $\phi_h$ can be tuned by changing carrier energy and/or strain, e.g., $\phi_h \simeq \pm 40°$ for valleys $D$ and $D'$ in the case of $\varepsilon = 0.3$ eV and $\sigma = 3\%$ presented here. This property can be an important ingredient for controlling directional currents and highly focused beams. Note that in graphene $p$-$n$ junctions, only the beams around $\phi = 0$ are highly transmitted while the transmission is low for large angles, especially when the transition length between highly doped regions is large [15]. This essentially limits the performance of corresponding electronic-optics devices, especially at high temperature [19]. Moreover, when injected into the graphene-GB system, carriers in one valley are totally reflected while partly for the other valley, implying that both transmitted and reflected beams are highly valley polarized. In $p$-$n$ junctions, these two beams can also be achieved but are valley unpolarized [15,18].

*Directionally separated currents.*—For practical perspectives, it is necessary to analyze the electrical currents, which are always measured at finite temperature, contributed by carriers with different energies and, importantly, which flow in different directions [19]. This analysis can be performed by rewriting the standard Landauer formula for the left-to-right current and then extracting these directional components. In particular, the conductance can be computed as $G = \int_{-\pi/2}^{\pi/2} [\mathcal{G}_D(\phi_2) + \mathcal{G}_{D'}(\phi_2)] \cos \phi_2 d\phi_2$ with

$$\mathcal{G}_{D,D'}(\phi_2) = \frac{e^2}{\pi h} \frac{W}{\hbar v_F} \int \mathcal{T}_{D,D'}(\epsilon, \phi_2) \left(-\frac{\partial f(\epsilon)}{\partial \epsilon}\right) |\epsilon| d\epsilon, \quad (2)$$

where $W$ denotes the width of the graphene sheet and $f(\epsilon)$ is the Fermi distribution function. Thus, the left-to-right current is the sum of contributions of all components flowing in different directions. In practice, these directional currents can be experimentally measured using multiple directional leads [10,11,18,19,23–26], as diagrammatically simplified in Fig. 4(e). Actually, the directional currents partly contribute to the left-to-right one measured at the right lead and partly reach the leads $T$ and $B$, depending on their intensity and direction.

In Fig. 4(a), conductances $\mathcal{G}_{D,D'}(\phi_2)$ computed using Eq. (2) and valley polarization $P_{val} = (\mathcal{G}_D - \mathcal{G}_{D'})/(\mathcal{G}_D + \mathcal{G}_{D'})$ at different temperatures are presented. Actually, directionally separated currents with nearly perfect $P_{val}$ and high intensity around the directions $\phi_2 = -\phi_h \approx \mp 40°$ (for valleys $D$ and $D'$, respectively) are achieved even at 300 K. Complete pictures showing the dependence of $\mathcal{G}_{D,D'}$ and $P_{val}$ on the Fermi level $E_F$ are also displayed in Figs. 4(b)–4(d). As discussed above, when varying $E_F$ (e.g., by tuning a back gate voltage [19]), the direction $\phi_h$
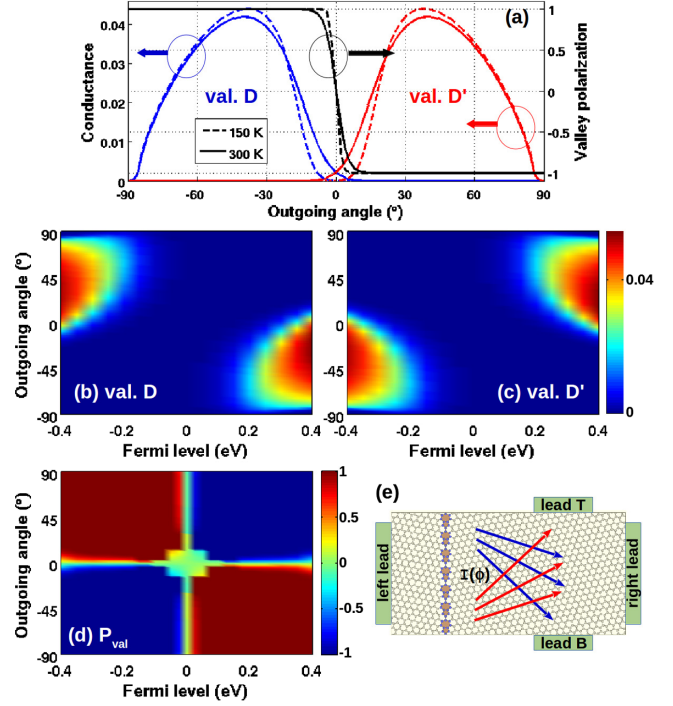


FIG. 4. (a) Conductance $\mathcal{G}_{D,D'}$ (left axis) in unit of $(2e^2W/3\pi ha_0)$ ($a_0 = 1.42$ Å) and valley polarization $P_{val}$ (right axis) as a function of outgoing angle $\phi_2$ for Fermi level $E_F = 0.3$ eV and at different temperatures. ($E_F$, $\phi_2$) maps of (b),(c) $\mathcal{G}_{D,D'}$ and (d) $P_{val}$ at 300 K. All data were obtained for $\sigma = 3\%$ in the GB1 system. (e) Simple schematic of multiple electrode devices for measuring the directional currents.

of high intensity current can be easily modulated as it moves to small angles when increasing $E_F$ and vice versa. Most importantly, the well-separated currents and high $P_{val}$ can be observed at room temperature and in a wide range of $E_F$ as shown for $|E_F| \leq 0.4$ eV here.

Remarkably, when changing from electrons to holes, $\mathcal{G}_{D,D'}$ reverse their direction [see Figs. 4(b) and 4(c)]. Accordingly, $P_{val}$ reverses its sign [see Fig. 4(d)]. This feature is essentially a consequence of the fact that the group velocity of electrons (holes) is parallel (antiparallel) to the momentum. This leads to a change in the sign of $\phi_{1,2}$ as described in Eq. (1) when applied to hole transport. With the gate tunability of $E_F$ [17–19], this property offers an excellent possibility of gate controlling the valley-polarized currents in considered devices.

Finally, though the effects of scattering at grain boundaries on the transmission function are strongly dependent on their atomic structure (e.g., see Fig. 2), our calculations show that the properties discussed above should be common to all periodic grain boundaries.

In conclusion, polycrystalline graphene, when subjected to strain, has been demonstrated to be a very promising candidate for manipulating highly valley-polarized currents and optical-like behaviors of massless Dirac fermions with novel refraction rules. Interestingly, the predicted

properties are observable at room temperature, in a wide range of incident angle and energy, and gate controllable. Although limited to the periodic grain boundaries, the study presents several practical perspectives. Generally, the disorder at grain boundaries could affect the $k_y$ conservation and hence induce a leakage current within the transmission gaps. However, some efforts to achieve periodic grain boundaries at large scale have been experimentally realized [23,27,28]. In particular, periodic grain boundaries as long as a few tens of nanometers can be obtained after thermal reconstruction of aperiodic ones [28]. Otherwise, a weak disorder is expected to not strongly affect the transport properties observed in periodic systems; see, e.g., Refs. [29,40]. Following the basic principles, momentum conservation and mismatch of electronic properties between different crystalline domains, our general approach can be extended to other polycrystalline systems of different materials including 2D layered, thin films and 3D materials [31,32].

---

*viet-hung.nguyen@uclouvain.be

[1] A. H. Castro Neto, F. Guinea, N. M. R. Peres, K. S. Novoselov, and A. K. Geim, Rev. Mod. Phys. **81**, 109 (2009).

[2] A. C. Ferrari *et al.*, Nanoscale **7**, 4598 (2015).

[3] J. R. Schaibley *et al.*, Nat. Rev. Mater. **1**, 16055 (2016); P. Makk, Nat. Phys. **11**, 894 (2015).

[4] Y. P. Shkolnikov, E. P. De Poortere, E. Tutuc, and M. Shayegan, Phys. Rev. Lett. **89**, 226805 (2002); K. Takashina, Y. Ono, A. Fujiwara, Y. Takahashi, and Y. Hirayama, Phys. Rev. Lett. **96**, 236801 (2006); D. Xiao, G.-B. Liu, W. Feng, X. Xu, and W. Yao, Phys. Rev. Lett. **108**, 196802 (2012).

[5] A. Rycerz, J. Tworzydło, and C. W. J. Beenakker, Nat. Phys. **3**, 172 (2007).

[6] D. Xiao, W. Yao, and Q. Niu, Phys. Rev. Lett. **99**, 236809 (2007).

[7] D. Gunlycke and C. T. White, Phys. Rev. Lett. **106**, 136806 (2011).

[8] Z. Wu, F. Zhai, F. M. Peeters, H. Q. Xu, and K. Chang, Phys. Rev. Lett. **106**, 176802 (2011); Y. Jiang, T. Low, K. Chang, M. I. Katsnelson, and F. Guinea, Phys. Rev. Lett. **110**, 046601 (2013); J. L. Garcia-Pomar, A. Cortijo, and M. Nieto-Vesperinas, Phys. Rev. Lett. **100**, 236801 (2008).

[9] S. H. Hsieh and C. S. Chu, Appl. Phys. Lett. **108**, 033113 (2016).

[10] R. V. Gorbachev *et al.*, Science **346**, 448 (2014).

[11] M. Sui *et al.*, Nat. Phys. **11**, 1027 (2015); Y. Shimazaki, M. Yamamoto, I. V. Borzenets, K. Watanabe, T. Taniguchi, and S. Tarucha, Nat. Phys. **11**, 1032 (2015).

[12] K. I. Bolotin, K. J. Sikes, Z. Jiang, M. Klima, G. Fudenberg, J. Hone, P. Kim, and H. L. Stormer, Solid State Commun. **146**, 351 (2008); A. S. Mayorov *et al.*, Nano Lett. **11**, 2396 (2011).

[13] P. Darancet, V. Olevano, and D. Mayou, Phys. Rev. Lett. **102**, 136803 (2009).

[14] V. V. Cheianov, V. Fal'ko, and B. L. Altshuler, Science **315**, 1252 (2007).

[15] P. E. Allain and J. N. Fuchs, Eur. Phys. J. B **83**, 301 (2011).

[16] Q. Wilmart, S. Berrada, D. Torrin, V H. Nguyen, G. Fève, J.-M. Berroir, P. Dollfus, and B. Plaçais, 2D Mater. **1**, 011006 (2014).

[17] J. R. Williams, T. Low, M. S. Lundstrom, and C. M. Marcus, Nat. Nanotechnol. **6**, 222 (2011).

[18] P. Rickhaus, R. Maurand, M.-H. Liu, M. Weiss, K. Richter, and C. Schönenberger, Nat. Commun. **4**, 2342 (2013); Appl. Phys. Lett. **107**, 251901 (2015); Nano Lett. **15**, 5819 (2015).

[19] G.-H. Lee, G.-H. Park, and H.-J. Lee, Nat. Phys. **11**, 925 (2015); S. Chen *et al.*, Science **353**, 1522 (2016).

[20] L. P. Biró and P. Lambin, New J. Phys. **15**, 035024 (2013).

[21] O. V. Yazyev and Y. P. Chen, Nat. Nanotechnol. **9**, 755 (2014).

[22] A. W. Cummings, D. L. Duong, V. L. Nguyen, D. Van Tuan, J. Kotakoski, J. E. B. Vargas, Y. H. Lee, and S. Roche, Adv. Mater. **26**, 5079 (2014).

[23] Q. Yu *et al.*, Nat. Mater. **10**, 443 (2011).

[24] A. W. Tsen, L. Brown, M. P. Levendorf, F. Ghahari, P. Y. Huang, R. W. Havener, C. S. Ruiz-Vargas, D. A. Muller, P. Kim, and J. Park, Science **336**, 1143 (2012).

[25] P. Yasaei *et al.*, Nat. Commun. **5**, 4911 (2014).

[26] V. Kochat, C. S. Tiwary, T. Biswas, G. Ramalingam, K. Hsieh, K. Chattopadhyay, S. Raghavan, M. Jain, and A. Ghosh, Nano Lett. **16**, 562 (2016).

[27] J.-H. Chen, G. Autes, N. Alem, F. Gargiulo, A. Gautam, M. Linck, C. Kisielowski, O. V. Yazyev, S. G. Louie, and A. Zettl, Phys. Rev. B **89**, 121407(R) (2014).

[28] B. Yang, H. Xu, J. Lu, and K. P. Loh, J. Am. Chem. Soc. **136**, 12041 (2014).

[29] O. V. Yazyev and S. G. Louie, Nat. Mater. **9**, 806 (2010).

[30] V. H. Nguyen, T. X. Hoang, P. Dollfus, and J.-C. Charlier, Nanoscale **8**, 11658 (2016).

[31] T. H. Ly *et al.*, ACS Nano **8**, 11401 (2014); L. Vincent, G. Patriarche, G. Hallais, C. Renard, C. Gardès, D. Troadec, and D. Bouchier, Nano Lett. **14**, 4828 (2014); A. Stoffers, B. Ziebarth, J. Barthel, O. Cojocaru-Miredin, C. Elsasser, and D. Raabe, Phys. Rev. Lett. **115**, 235502 (2015); Y. Liu, Y. Y. Li, S. Rajput, D. Gilks, L. Lari, P. L. Galindo, M. Weinert, V. K. Lazarov, and L. Li, Nat. Phys. **10**, 294 (2014).

[32] V. H. Nguyen, H.-V. Nguyen, J. Saint-Martin, and P. Dollfus, Nanotechnology **26**, 115201 (2015); Y. Wang *et al.*, Adv. Funct. Mater. **25**, 68 (2015); J. R. Wallbank *et al.*, Science **353**, 575 (2016).

[33] L. Lindsay and D. A. Broido, Phys. Rev. B **81**, 205441 (2010).

[34] V. M. Pereira, A. H. Castro Neto, and N. M. R. Peres, Phys. Rev. B **80**, 045401 (2009).

[35] See Supplemental Material at http://link.aps.org/supplemental/10.1103/PhysRevLett.117.247702, which includes Refs. [36–39]. In this material, the validity of our tight-binding calculations, compared to the first-principles

PHYSICAL REVIEW LETTERS

methods, is demonstrated and the transport properties of incommensurable systems are discussed.

[36] X. Gonze *et al.*, Comput. Phys. Commun. **180**, 2582 (2009).

[37] http://www.openmx-square.org.

[38] J. Sun, N. Lin, Z. Li, H. Ren, C. Tang, and X. Zhao, RSC Adv. **6**, 1090 (2016).

[39] A. Lherbier, S. M.-M. Dubois, X. Declerck, Y. M. Niquet, S. Roche, and J. C. Charlier, Phys. Rev. B **86**, 075402 (2012).

[40] P. Vancsó, G. I. Márk, P. Lambin, A. Mayer, C. Hwang, and L. P. Biró, Appl. Surf. Sci. **291**, 58 (2014); H. Zhang, G. Lee, C. Gong, L. Colombo, and K. Cho, J. Phys. Chem. C **118**, 2338 (2014).